

LIVE-GS: LLM Powers Interactive VR by Enhancing Gaussian Splatting

Haotian Mao*
Shanghai Jiao Tong University

Yule Quan§
Shanghai Jiao Tong University

Zhuoxiong Xu†
Shanghai Jiao Tong University

Nianchen Deng¶
Shanghai AI Lab

Siyue Wei‡
Shanghai Jiao Tong University

Xubo Yang||
Shanghai Jiao Tong University

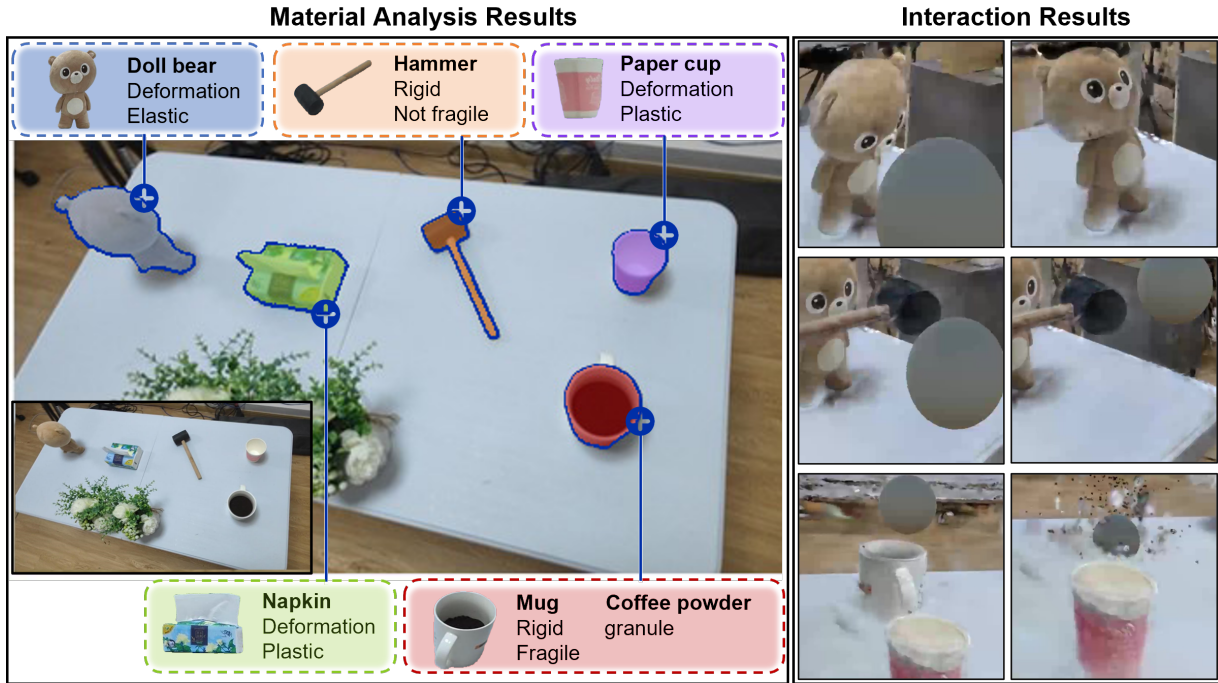


Figure 1: Our system, LIVE-GS, reconstructs the scene with extra features and segments target objects. Most importantly, our GPT-powered system is capable of analyzing their physical properties, thus guiding simulations consistent with real phenomena. When we throw balls at them, the doll swings and the mug is broken, while the ball will bounce when hitting the hammer.

ABSTRACT

Recently, radiance field rendering, such as 3D Gaussian Splatting (3DGS), has shown immense potential in VR content creation due to its high-quality rendering and efficient production process. However, existing physics-based interaction systems for 3DGS can only perform simple and non-realistic simulations or demand extensive user input for complex scenes, primarily due to the absence of scene understanding. In this paper, we propose LIVE-GS, a highly realistic interactive VR system powered by LLM. After object-aware GS reconstruction, we prompt GPT-4o to analyze the physical properties of objects in the scene, which are used to guide physical simulations consistent with real phenomena. We also design a GPT-assisted GS inpainting module to fill the unseen area covered by manipulative objects. To perform a precise segmentation of Gaus-

sian kernels, we propose a feature-mask segmentation strategy. To enable rich interaction, we further propose a computationally efficient physical simulation framework through an PBD-based unified interpolation method, supporting various physical forms such as rigid body, soft body, and granular materials. Our experimental results show that with the help of LLM’s understanding and enhancement of scenes, our VR system can support complex and realistic interactions without additional manual design and annotation.

Index Terms: 3D gaussian splatting, virtual reality, physical-based modeling, material analysis

1 INTRODUCTION

With swift advancement of virtual and augmented reality technologies, increasingly realistic and reliable immersion have emerged, leading to numerous applications in education, healthcare and assembly training. In addition to traditional modeling techniques, radiance field rendering has demonstrated enormous potential in VR asset creation due to its remarkable novel synthesis capabilities. In the era of neural radiance fields (NeRF) [31], various methods have been developed to enhance its rendering efficiency in VR [5, 53]. However, NeRFs face challenges with physics-based dynamic due to its implicit representations.

With rapid evolution, 3D Gaussian Splatting(3DGS) [21] has

*e-mail: maohaotian@sjtu.edu.cn

†e-mail: vector-02@sjtu.edu.cn

‡e-mail: weisiyue071024@sjtu.edu.cn

§e-mail: qyl728@sjtu.edu.cn

¶e-mail: dengnianchen@pjlab.org.cn

||e-mail: yangxubo@sjtu.edu.cn

quickly taken precedence for its real-time efficiency and seamless integration with modern rasterization pipeline. Its point cloud format, enriched with geometry information, also facilitates particle-based approaches for physical simulations. VR-GS [19] successfully implements the first interactive physics-based VR system based on 3DGS, showing its potential for interactive VR scene reconstruction. However, their method limits interactions to elastic deformation, which may result in unrealistic experiences. Although approaches like Physdreamer [62] attempt to reconstruct physical properties, they are constrained by pre-assumptions and struggle with complex real-world scenes. Currently, there is a lack of a VR system capable of analyzing physical properties and enabling real-time interaction in scenarios involving various materials, which becomes more challenging in real-world environments.

To address these limitations, we introduce LIVE-GS, an interactive VR system based on 3DGS, which is capable of performing physical property analysis tasks. Leveraging GPT models, our system exhibits strong scene understanding capabilities, enabling it to determine and analyze the physical properties of objects from minimal input images. Our system aims to reconstruct complex real-world scenes and facilitate real-time interactions consistent with actual phenomena. Therefore, inspired by skinning algorithms [20, 28], we implement a unified physical simulation method based on PBD [32], which supports various types of simulation such as deformation, fracture and granular material while maintaining high efficiency. To extract simulation target from the whole scene, we design a feature-mask strategy, combining identity features and masks to segment targets precisely. To further improve immersion, we also utilize GPT to enhance existing tracking techniques [3] to detect generated artifacts in unseen regions after removal, which can be used to guide fine-tuning stage with 2D inpainting technique LaMa [45].

We compare our segmentation and physical simulation with previous methods, demonstrating that our system achieves competitive results in simulation quality and real-time efficiency for VR interactions. We also present several VR demos from public and custom datasets, showcasing the effectiveness of our material analysis technique and scene reconstruction abilities.

In conclusion, our major contributions can be summarized as follows:

- LIVE-GS, a highly realistic interactive VR system with LLM-powered scene enhancement, capable of analyzing physical properties and ensuring interactions consistent with scene semantics.
- A feature-mask segmentation method in GS scene, achieving accurate identification of boundaries for object-level segmentation, which facilitates interactive manipulation.
- A particle interpolation method for GS physical simulation, which is fast and supports various physical phenomena such as deformation, fracture, and granular material.

2 RELATED WORK

2.1 3D Gaussian Splatting

In the field of novel view synthesis, 3D Gaussian Splatting [21] has recently emerged, achieving remarkable real-time rendering with splat-based rasterization. Subsequent work simultaneously expands its applicability and capabilities. Original 3DGS neglects the underlying geometry information, leading to redundant Gaussian kernels, which limits the rendering speed in large scenes. [29, 40] are devoted to dynamically guiding the distribution and rendering of kernels, achieving high quality without sacrificing efficiency. Besides, it complicates the recovery of accurate surfaces (mesh) with irregular arrangement, where [13, 51, 10, 49, 9] import depth

and normal supervision for surface-aligned results. For object-level segmentation, SAGD [15] proposes a boundary-enhanced segmentation pipeline by lifting a 2D foundation model with training, while many other work supplements additional identity features [7, 43, 56, 2, 50] during the training procedure. However, void-like hole defects can be exposed after object removal caused by lacking of information. A common way to tackle this problem is leveraging 2D inpaint guidance [56] for fine-training, and depth priors greatly benefit this procedure [27, 16]. Furthermore, this technique can be extended to dynamic scenes such as video reconstruction [4, 1], deformation field reconstruction [14, 8, 55, 17] and diffusion-based content creation [24, 57, 39]. These jobs are inspiring for our scene reconstruction and interaction.

2.2 Scene Understanding

Scene understanding is essential in 3D scene generation and reconstruction. Many researches have investigated in aligning visual and language presentation such as CLIP [38], DINO [60] and ALIGN [18]. The development of these models has led to breakthrough in scene understanding tasks. Many works [22, 3, 6, 30, 34, 46] develop pre-trained promptable models handling various object detection and segmentation problems on arbitrary data. Recently, further researches thoroughly investigate multi-modal capabilities for various scene information such as video, text and audio [59, 54, 11, 61].

In radiance field, many works have been done to achieve high-quality rendering and consistency across different views. Feature field distillation has been well explored in some NeRF-related work such as [63] and [42]. Another stream of methods obtain semantic embeddings from pre-trained models for open-vocabulary 3d scene understanding [42, 26]. 3DGS can also obtain semantic embeddings via optimization in similar way [41, 64, 36, 25, 41]. Inspired by previous researches, we design an image-based material analysis strategy based on GPT-4o in our system, thus achieving a scene reconstruction consistent with visual effects.

2.3 Physical Simulation in Radiance Field

In the era of NeRF, its physics-based application in VR has been strictly hindered by its implicit expression. Some works related to physics-based deformation [35, 58] relies on extracted mesh. Although several researches have achieved physical dynamics of complex particle systems [12, 23], it is challenging to integrate into VR application due to such significant computational overload. Since 3DGS was published, its point cloud based representation has been explored for various physical-based applications. PhysGaussian [52] integrates physical principles based on MPM into the rendering process, enabling realistic dynamics for different materials. Feature splatting [37] proposes a language-grounded method in physical engine, including physically realistic movement and scene editing. PhysDreamer [62] reconstructs material field of static objects with the assistance of video generation model, enhancing engagement of virtual experience. For real-time simulation and interaction in VR scene, VR-GS [19] implements a comprehensive reconstruction system and a physical engine based on PBD. Leveraging prior researches, our work proposes a unified interpolation method based on PBD, supporting various real-time physics-based simulations and interactions such as deformation, fracture, and granular material.

3 METHOD

In this section, we introduce our pipelines in three parts as shown in figure 2: instance-aware scene reconstruction, GPT-powered scene enhancement and interactive physical simulation framework. Through our pipeline, our system constructs the scene with 3DGS, labels every object, segments them and assigns physical properties based on analysis results, achieving high-efficiency interactions in VR.

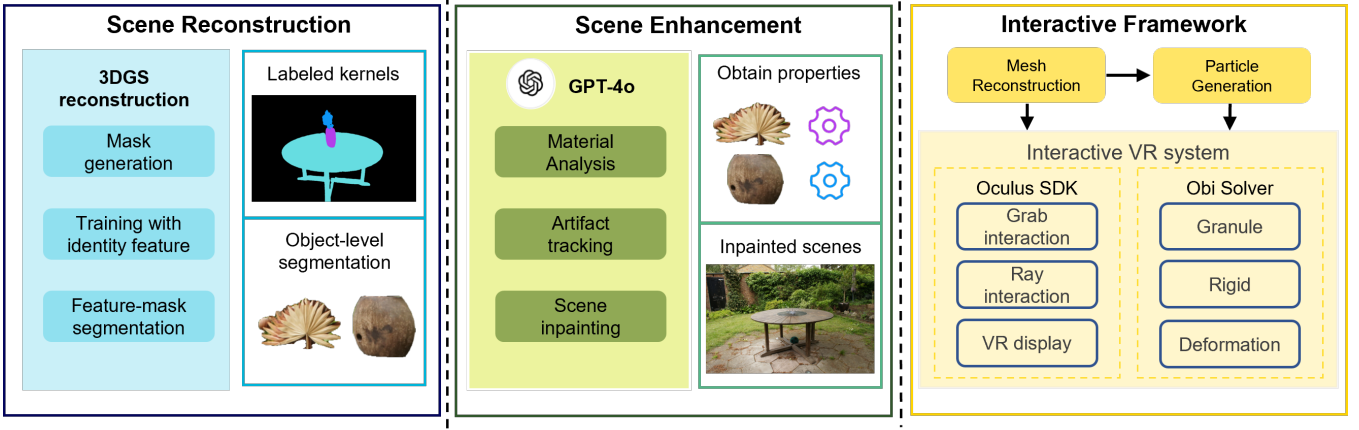


Figure 2: **System overview.** Our system consists of three parts: scene reconstruction, scene enhancement and interactive framework. With original images and initial point clouds, we train Gaussian model with identity encoding and segment our targets through feature-mask segmentation. Afterwards, we leverage GPT to enhance our system’s scene understanding by analyzing objects’ properties and tracking possible artifacts caused by object removal. We import another fine-tuning stage to inpaint possible artifacts. Finally, we implement our GS-based VR system with Oculus SDK and Obi solver, achieving immersive real-time interactions.

3.1 Instance-aware Scene Reconstruction

Gaussian training with identity encoding 3DGS[21] represents a scene using a collection of colored 3D Gaussians and renders them into camera views through splatting-based rasterization. Each 3D Gaussian primitive is characterized by its center \mathbf{p}_k and covariance matrix Σ_k :

$$G_k = \exp\left(-\frac{1}{2}(\mathbf{x} - \mathbf{p}_k)^T \Sigma_k^{-1} (\mathbf{x} - \mathbf{p}_k)\right), \quad (1)$$

where \mathbf{x} is an arbitrary position in world space and the covariance matrix $\Sigma = RSS^T R^T$ is formulated by scaling matrix S and rotation matrix R . Additionally, each Gaussian kernel carries an opacity α and a color c for tile-based rasterization. 3D Gaussian kernels G_k are first transformed to image plane as 2D Gaussian kernels G' [65], and then input for sorting and volumetric alpha blending:

$$C = \sum_i^N c_i \delta_i \prod_{j=1}^{i-1} (1 - \delta_j), \delta_i = \alpha_i G'_i(x') \quad (2)$$

where x' represents the target pixel, whose rendering result is influenced by N Gaussian kernels.

Starting from a set of images to produce a sparse point cloud with SfM method[44], learnable parameters are optimized end-to-end through photometric loss. Furthermore, in case over-skinny kernels generate prickly artifacts under deformations, we introduce anisotropy loss from [52]:

$$\mathcal{L}_A = \frac{1}{|G|} \sum_{G_i \in G} \max\{\max(S_{G_i})/\min(S_{G_i}), r\} - r \quad (3)$$

which constrains the ratio between maximum and minimum axis in scaling parameter. Accordingly, total image loss becomes:

$$\mathcal{L}_I = (1 - \lambda_1)\mathcal{L}_1 + \lambda_1\mathcal{L}_{SSIM} + \mathcal{L}_A \quad (4)$$

To segment each interactive object, we add additional identity features to each kernel and jointly train them offline. We first deploy SAM [22] to generate masks automatically, then take DEVA [3] to obtain consistent mask labels across training views as ground

truth. For enhanced robustness and accuracy, grouping loss, including **2D identity loss** and **3D regularization loss**, is introduced from Gaussian Grouping[56]:

$$\mathcal{L}_G = \lambda_{2d}\mathcal{L}_{2d} + \lambda_{3d}\mathcal{L}_{3d} \quad (5)$$

Therefore, final loss function becomes:

$$\mathcal{L} = \mathcal{L}_I + \mathcal{L}_G \quad (6)$$

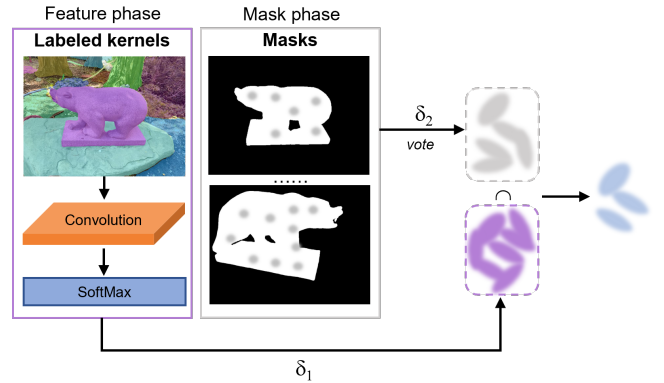


Figure 3: **Feature-mask segmentation.**

Feature-mask segmentation To segment objects from environments for subsequent processing, we design a feature-mask method, which is divided into two stages: *feature stage* and *mask stage*, for accurate segmentation. We choose the intersection of results in two stages as outcome.

Feature Stage: During training procedure, we import a classifier C along with 3D regularization loss, which we use to calculate the attribution of each kernel. With predefined threshold σ_1 , each kernel k of object i is segmented by:

$$\{k | \text{Softmax}(C(k, i)) > \sigma_1\} \quad (7)$$

This stage is robust to masks generated from DEVA, ensuring correctness even in the presence of minor errors. However, it is relatively aggressive because redundant kernels would be peeled from

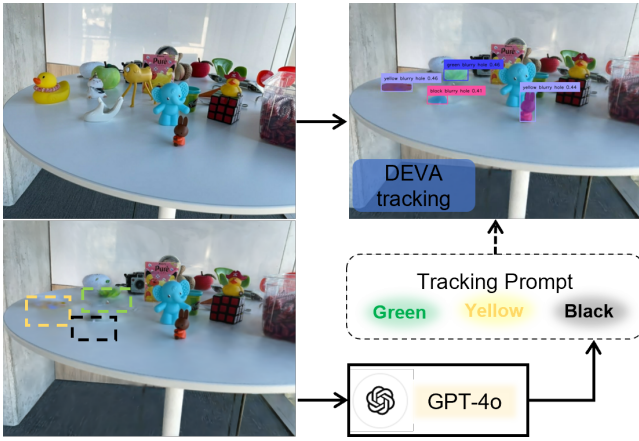


Figure 4: **Artifacts tracking.** We input the source image, the removal image and related mask in GPT-4o to obtain color prompts. Then we track the artifacts with DEVA and intersect them with the mask, generating the final mask for 2D inpainting method.

the environment. The result is far beyond our requirement for subsequent simulation.

Mask Stage: To obtain fine segmented result, we adopt a voting strategy similar to [15]. We project each kernel to screen space recorded as G'_k and determine whether its center is inside corresponding mask. With mask M_j of each view j obtained from DEVA, we set vote as:

$$V(i, j, k) = \begin{cases} 1, & G'_k \text{ in } M_i \\ 0, & G'_k \text{ not in } M_i \end{cases} \quad (8)$$

We calculate the proportion passed in total count n :

$$P(i, k) = \sum_{j=0}^{n-1} V(i, j, k) / n \quad (9)$$

and assign kernel k to object i if $P(i, k)$ exceeds the threshold σ_2 . Considering the possible incompleteness when obtaining each mask, we choose a relatively low threshold during this stage, in case we lose our target objects.

3.2 GPT-powered Scene Enhancement

In this section, we introduce our strategy to leverage GPT to enhance the scene understanding of our system, which consists of **material analysis** and **artifact tracking**.

Material Analysis In our system, we intend to restore the material property according to input images. PhysDreamer [62] optimizes the differentiable material field based on video generation priors for elastic objects, but it is hard to extend to more materials. Instead, we use GPT-4o for material analysis due to its strong visual perception capabilities. Considering that the environment is important for analysis, we input two images: the first one is the original image and the other is the mask marking the target for analysis. The model is demanded to output formatted reply such as *json* file, which is strongly connected with our underlying physical engine. We demand the model to distinguish among deformation, granular material and rigid, estimating their properties. These can be summarized into two categories: **object property** and **particle property**.

Object property This kind of property is volume dependent, which is also represented by the number of particles. We mainly

choose **mass** and demand the system to give concrete value. However, our image-based analysis is affected by the perspective transformation where distant objects look small on the screen space, hence leading to lower values. More seriously, since all particles in one object share equally the whole mass, each particle is allocated little mass in an object with plenty of particles. If small values are given, it will suffer from unstable numerical calculation. Therefore, instead of applying them directly into our engine, we supplement an correction factor C to resolve above problems:

$$C = aM, \quad (10)$$

$$M = \begin{cases} \sqrt[3]{N_p} & , \text{ for granular and deformable material} \\ \sqrt{N_p} & , \text{ for rigid} \end{cases}$$

This factor is proportional to the cube root of the particles numbers N_p in *deformation* and *granular material* and square root in *rigid* due to their voxel and surface particle generation strategies respectively.

Particle property This kind of property is related with constraints between particles, which is independent of the object size. These values are required to be normalized, which favours the judgement of our system. These attributes are then converted proportionally in certain ranges and input into our system.

1) Deformation

- *Deformation Resistance.* This shows the degree of the deformation under stress. When receiving the same force, the object with bigger resistance value will produce smaller deformation.
- *Plasticity.* Objects with stronger plasticity can absorb more force without turning back to original shapes.

2) Granular material

- *Friction.* This affects forces that particles impose on their neighborhood, thus influencing their movement.

3) Rigid

- *Fragility.* This attribute marks whether it can be broken when affected by external forces.
- *Force Threshold.* If the object is fragile, this value means the maximum force it can endure.

Our analysis is achieved through prompt engineering with few-shot trick, while web search is enabled to obtain richer knowledge for better understanding. We also add dialogue prompt for users to appoint specific material, which especially favours our experiments in the next section. It is convenient to adjust the analysis for more properties or migrate between different physical engines.

Artifact tracking After training, Gaussian kernels mainly distributed on the surface in the scene, leaving unseen region empty. After object removal, unseen background may be exposed as artifacts especially for supporting surface, which strictly affects immersive experience in VR. To tackle this problem, we use 2D method LaMa [45] in multi-view to guide our inpainting training, which requires corresponding masks. Similar to segmentation stage, DEVA can be used to detect artifacts region, but many misjudgement may occur due to its vague language prompts. Therefore, we design a GPT-powered module to enhance its accuracy.

One way is to utilize GPT-4o to generate suitable prompts. We find that DEVA is sensitive to the color description, which can be related to the removed objects. Therefore, we use three images as input for GPT-4o: original scene I_o , scene after removal I_r and removal mask M_r , and require it to reply the concrete color. Furthermore, our feature-mask segmentation strictly constrains the removed part, so the artifacts can only appear inside M_r . Therefore,

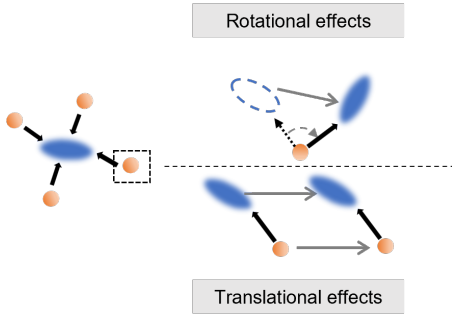


Figure 5: **Particle interpolation for Gaussian kernels.** The rotation of the particles not only contributes to the rotation quaternion but also affects the transition vector.

we calculate the intersection of M_r and the DEVA result as the final input M_f for LaMa.

We insert extra Gaussian kernels in removed region and freeze other kernels in fine-training stage. With each inpainted image I_p and original image I , we set Loss as:

$$L_f = L_1(I_p, M_f) + L_1(I, M_f) \quad (11)$$

where I_p is used to calculate loss inside M_p and I is used for the outside. Considering the irregularity of the mask, the SSIM loss is abandoned here for better results.

3.3 Interactive Physical Simulation Framework

For real-time rendering and interaction in VR system, we implement our simulation with PBD [32]. However, the number of Gaussian kernels in each segmented objects is usually enormous, which can largely increase the overload if they are directly converted for simulation. Therefore, we implement interpolation method similar with VR-GS [19] and extend it to more situations.

Firstly, we generate physical particles from object surfaces, which participate in physical calculation but keep invisible during rendering. Their changes in rotation and transition compared with initial state can be calculated and recorded as ΔR and ΔT . For each Gaussian kernel, we find the closest m particles and calculate their weights at frame 0, where m is determined by specific phenomenon. The weights should be related to the distance between the kernel and nearby particles at initialization as long as normalization is ensured. We choose the inverse of distance in this paper. Accordingly, the translation vector and rotation quaternion can be calculated as:

$$T' = \sum_i^{m-1} w_i \Delta T_i \quad R' = \sum_i^{m-1} w_i \Delta R_i \quad (12)$$

Additionally, the rotation of particles contributes to the translation vector, which can be calculated as follows:

$$X_i^d = X_{i,r} - X_{i,r}^p \quad T_q = \sum_i^{m-1} w_i (\Delta R_i X_i^d (\Delta R_i)^{-1} - X_i^d) \quad (13)$$

where X_i^d expresses the vector between the kernel and its relevant particles when starting. It can be calculated at initialization for better rendering efficiency. With above calculation, the runtime position and rotation can be calculated as:

$$T = T_r + T' + T_q \quad R = R_r + R' \quad (14)$$

we choose $m = 4$ for elastic objects to achieve smooth simulation, while $m = 1$ is enough for granular material and rigid. To better exhibit our results, we also implement fracture for rigid.

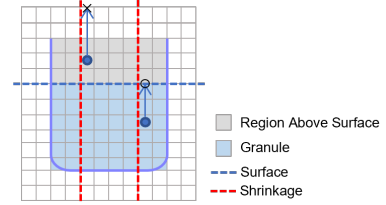


Figure 6: **Particles filling in container.** *six detections* fail in the region above the surface but *five detections* can succeed. Filling particles find the nearest surface in the shrinkage and inherit their attributes.

For granular material, we choose a more common condition based on realistic situation, where it is in some containers and Gaussian kernels only distribute on the surface. To completely reconstruct it, we refer to internal filling method in PhysGaussian [52] and improve it for our target. The core is to obtain kernels of the surface when inheriting relevant attributes and separate the container from the content. Instead of simply casting rays along six axes to search for internal region, we supplement another detecting strategy in five directions for regions above the powder. As shown in figure 6, voxels in the boundary of these two regions are recognized as the surface, in which the Gaussian kernels are extracted as granules with filling kernels. In case the container is extracted accidentally, we add shrinkage parameter for the bounding box, thus only using the surface at the middle of the container. Furthermore, we find that kernels at surface usually have large scale, which causes blurry rendering and excessive overlapping when simulating, hence a scaling factor s_f is added to control this. Besides, the anisotropy is eliminated by minimum axis length to avoid prickly shape:

$$S_i = \min(S) \quad \text{for } i = \{1, 2, 3\} \quad (15)$$

4 EXPERIMENTS

In this section, we describe the implementation details of our system and demonstrate our evaluation through several datasets. We present several interactive VR demos, measuring the real-time performance and comparing the realism with previous approaches.

4.1 Implementations

Our training code is built on Gaussian-grouping [56], where we use DEVA [3] to track and generate mask. We construct our material analysis part with langchain framework [48]. For physical simulation and interaction in VR, we build our underlying physical system based on Obi solver [47] in Unity 2022.3.30. Obi requires mesh for particle generation. So we use Open3D to construct mesh, which directs the particle generation for each segmented object. We only allow particles adsorbed on the surface for rigid, while voxel generation is turned on to fill the deformation and granular material. When generating particles, we choose a fixed density (particle numbers in each voxel or surface) for all simulations. Significantly, we raise the granular particle density to the upper limit to achieve better simulation results. Besides, the mesh enables collision detection in our system. To better fit the scene, we adopt plane fitting at supporting plane. We also implement distance field to achieve efficient detection.

In training stage, we choose $\lambda_1 = 0.2$ for image loss and $\lambda_{2d} = 1, \lambda_{3d} = 2$ for grouping loss. All dataset is trained for 30000 iterations. But considering the training speed and memory usage, 3d loss is only enabled for first 5000 iterations. In feature-mask segmentation, we choose $\theta_1 = 0.3$ and θ_2 from 0.2 to 0.4 for object-level segmentation. In the inpainting stage, we train the scene with

another 10000 iterations while allowing density control for the first 5000 iterations, avoiding excessive Gaussian kernels.

Our system is tested on Intel(R) Core(TM) i9-14900K CPU with 64GB memory and a NVIDIA GeForce RTX 4080 SUPER GPU with 16GB. We conduct our VR experiments on Quest 3 equipment with controllers.

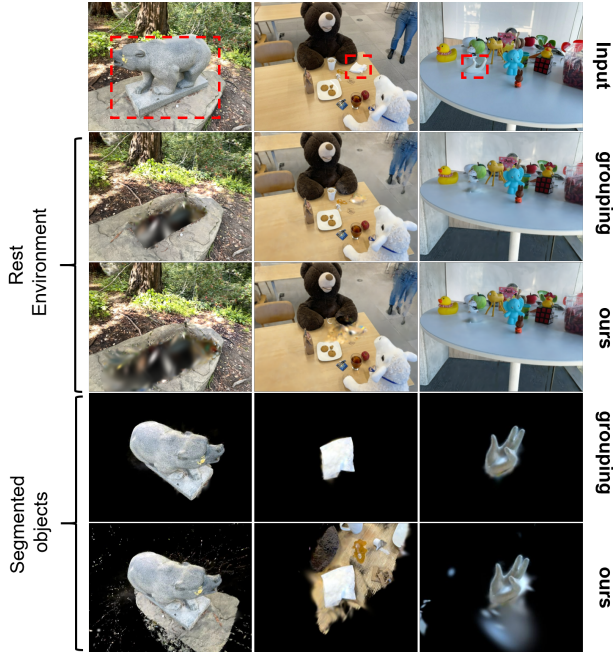


Figure 7: **Segmentation comparison with Gaussian-grouping.** We respectively render the images for removed objects and rest environment. Our method achieves detailed segmentation in various situation, which benefits the simulation.

4.2 Segmentation

The segmentation largely impacts the subsequent processing, especially for dynamic objects. We choose dataset *teatime*, *figurines* and *bear*, which consist of targets with different size. We compare our results with Gaussian-grouping, which only use identity feature for segmentation. Our results, including the target object and rest environment shown in figure 7, shows that our method achieves accurate results and avoids harming the rest environment, which is essential in scene reconstruction and simulation.

4.3 Physical Simulation

| Dataset | Frame time | Step time | PhysGaussian | Ours |
|---------|------------|-----------|--------------|------|
| wolf | 40 | 0.02 | 4060 | 221 |
| sofa | 20 | 0.1 | 397 | 150 |
| fox | 40 | 0.1 | 837 | 273 |

Table 1: Performance (time to generate one frame (ms)) : ours and PhysGaussian.

To prove the effectiveness of our simulation method, we choose dataset from PhysGaussian (*wolf*, *sofa*) [52] and Instant-NGP (*fox*) [33]. However, to guarantee visual consistence, the target could be recognized with different properties compared with the configuration in previous methods. Therefore, we use user prompts to explicitly appoint the material. For example, we input *wolf* images with "this wolf is made of sand" and *fox* with "this fox is a doll". For real analysis results, we will present them in the next section.

However, the Material Point Method (MPM) requires a tiny step for better simulation, which is typically unnecessary for PBD method. To benchmark the performance of our system, we align the frame time and step time with PhysGaussian in corresponding scenes, and measure the average time to generate each frame. As shown in table 1, our method outperforms in rendering efficiency. In real-time simulation, we set frame time to 0.02s and set substep to 4 iterations, which is sufficient for solving dynamic. We also compare our real-time simulation results with videos generated by PhysGaussian in figure 8. Although our method generates slightly different results due to underlying implementation, we still achieve competitive visual results. In the meantime, we achieve real-time rendering efficiency.

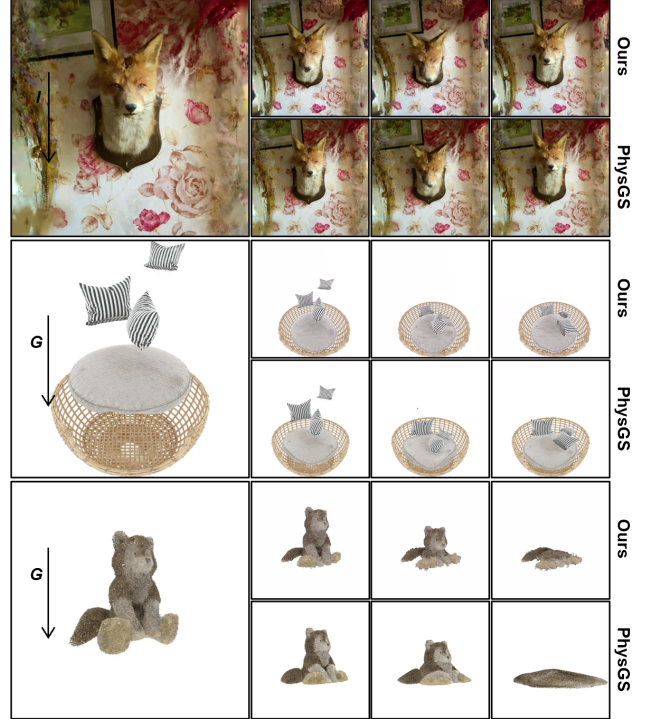


Figure 8: **Physical simulation compared with PhysGS.** We choose *fox*, *sofa* and *wolf* for our experiments. We achieve competitive simulation results while still maintaining high efficiency.

| <i>wolf</i> | Category | Mass (kg) | Friction | |
|-------------|-------------|-----------|------------------------|------------|
| 1 | granule | 0.5 | 0.3 | |
| <i>fox</i> | Category | Mass (kg) | Deformation Resistance | Plasticity |
| 1 | deformation | 0.5 | 0.3 | 0.2 |

Table 2: **Material analysis with prompt for fox and wolf.** In this way they act similar with PhysGS and we can interact with them.

4.4 Interactive Demos in VR

In this section, we evaluate our system with several interactive VR demos. We choose datasets from public data such as *garden* and previously mentioned *wolf*, *sofa*. We skip data *fox* here because it is analyzed as *rigid* and *unbreakable*, which cannot demonstrate interesting simulation results. In addition, we take our own datasets in real scenes with mobile phone, which includes about 260 photos. These datasets include various physical properties, which is suitable

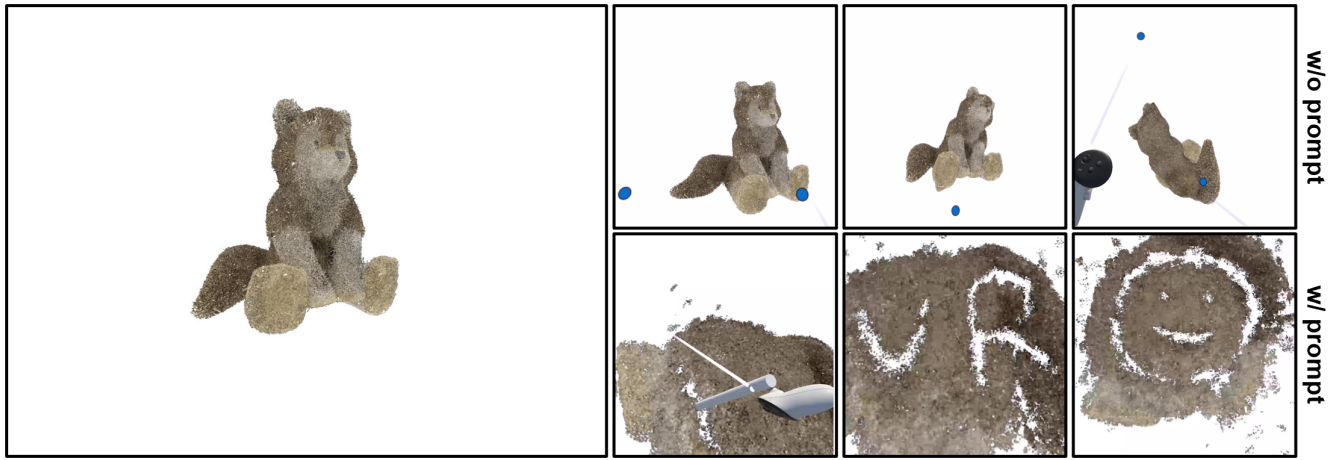


Figure 9: **Interaction with the wolf.** The first line is analyzed as a doll and we play with it. While the second line is analyzed as granular material like sand with dialogue prompt in comparison with PhysGS. We draw a VR and a smile on it.

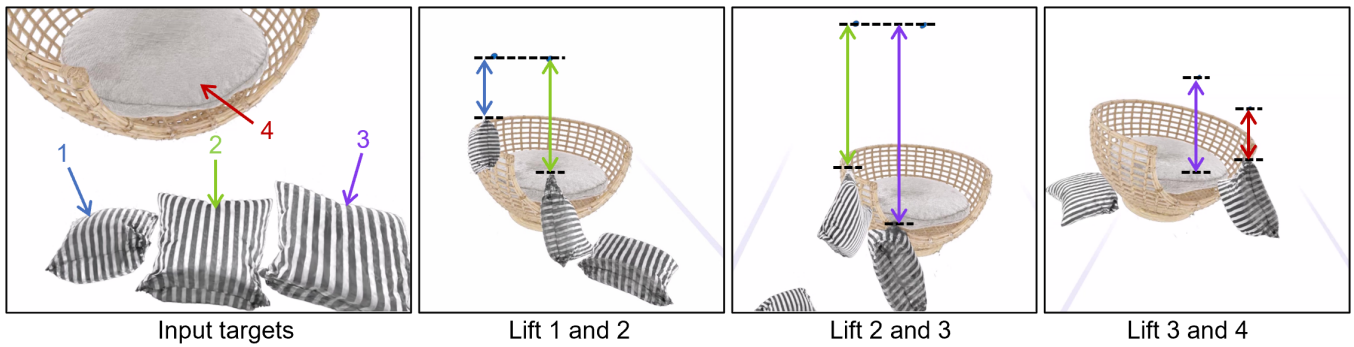


Figure 10: **Interaction in sofa.** We analyze the physical properties of pillows and cushion. Then we apply spring force to lift them up and two ends of the spring force are marked with arrows, observing the obvious distinction of their mass. Although predicted with the same mass values, they act aligned with visual effects after fixed by our correction factor.

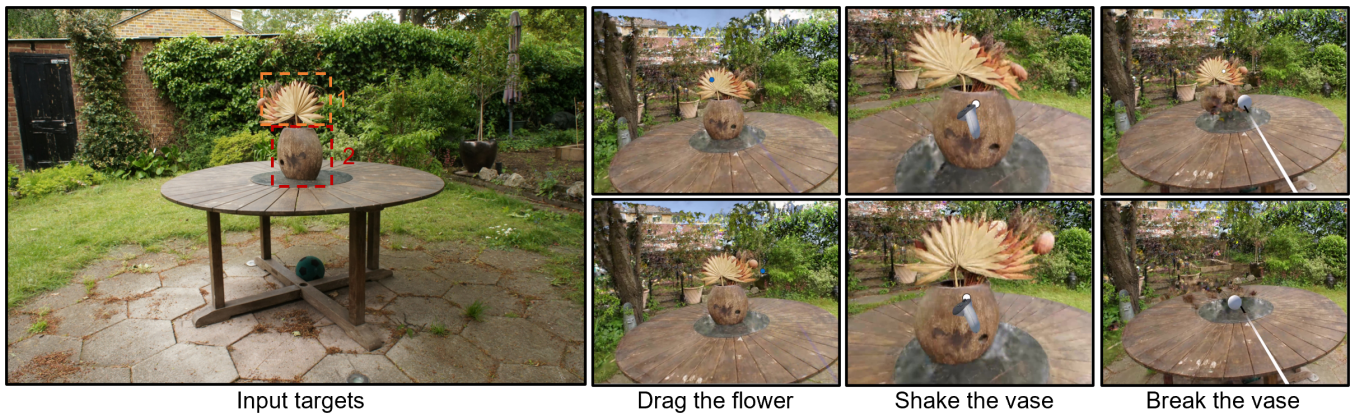


Figure 11: **Interaction in garden.** First, we drag the flower and shake the vase. Then we throw a ball, breaking the vase into pieces.

to test the material analysis ability and interaction in our system. We demonstrate our analysis details and complete particular tasks in each scene.

wolf and sofa In this section, we analyze the physical property without user dialogue for appointing. Different from Sec.4.3, the *wolf* here is recognized as a soft doll, which is consistent with our its visual effects. To fully demonstrate the difference, we play with

the *wolf* in different forms in our demos.

Pillows and cushion are also identified as *deformation*, but there is an obvious distinction in mass analysis. The cushion (number 4) is much heavier than the others, while the pillows are given the same value due to their similarity in perception. We apply a spring force on these objects in order to lift them up. With our adjustment method mentioned in Sec.3.2, the bigger pillow has more mass, thus

| <i>wolf</i> | Mass (kg) | Deformation Resistance | Plasticity |
|-------------|-----------|------------------------|------------|
| 1 | 0.3 | 0.2 | 0.5 |
| <i>sofa</i> | Mass (kg) | Deformation Resistance | Plasticity |
| 1 | 0.3 | 0.3 | 0.1 |
| 2 | 0.3 | 0.3 | 0.1 |
| 3 | 0.3 | 0.3 | 0.1 |
| 4 | 1.5 | 0.3 | 0.1 |

Table 3: Material analysis (both deformation) in *wolf* and *sofa*.

keeping the interactions consistent with visual effects.

Garden In this dataset, we segment the plant and the bottle respectively and analyze them. This demo reflects the strong scene understanding power of our material analysis, even when facing details in structured objects. The plant is recognized as **deformation** while the bottle is recognized as a *fragile rigid*. When we shake the bottle, the flower rotates with the base. Furthermore, we shoot a ball to the bottle to break it into pieces, and the flower falls onto the desk.

| Target | Category | Mass (kg) | Deformation Resistance | Plasticity |
|--------|-------------|-----------|------------------------|------------|
| 1 | deformation | 0.2 | 0.3 | 0.1 |
| Target | Category | Mass (kg) | Force threshold (N) | |
| 2 | rigid | 0.5 | 30 | |

Table 4: **Material analysis (both deformation) in *garden***. The plant is recognized as *deformation* while the bottle is recognized as *fragile rigid*.

Custom dataset *labdesk* To fully valid our system for the analysis and simulation of various material, we create our own datasets with multiple objects. The dataset consists of an empty paper cup, a mug with coffee powder, a plastic hammer, a doll bear and a box of tissues. The analysis result is shown as table 5. In this scene, users can enjoy various interesting interactions. When they try to drag the toy and the tissue, the toy always recover while the tissue may collapse due to their different levels of plasticity. They can also hold the hammer and break the mug, and the coffee powder splits out when broken.

| Target | Category | Mass (kg) | Deformation Resistance | Plasticity |
|--------|-------------|-----------|------------------------|------------|
| 1 | deformation | 0.05 | 0.2 | 0.8 |
| 2 | deformation | 0.2 | 0.3 | 0.5 |
| 3 | deformation | 0.3 | 0.4 | 0.2 |
| Target | Category | Mass (kg) | Force threshold (N) | Fragile |
| 4 | rigid | 0.5 | – | False |
| 5 | rigid | 0.3 | 20 | True |
| Target | Category | Friction | | |
| 6 | granule | 0.1 | | |

Table 5: **Material analysis in our own dataset *labdesk***. This scene contains various phenomena with different physical properties.

5 DISCUSSION AND FUTURE WORK

Segmentation. Segmentation is essential for reconstruction and simulation in GS scenes, especially when dealing with comprehensive real-world datasets. Our method focuses both on the remaining

| Scene | Gaussian kernels | particles | FPS w/o simulation | FPS in simulation |
|---------|------------------|-----------|--------------------|-------------------|
| wolf | 188201 | 350 | 129.0 | 105.8 |
| sofa | 636507 | 1477 | 104.7 | 62.0 |
| garden | 1843725 | 262 | 64.3 | 58.1 |
| labdesk | 1024703 | 6826 | 68.1 | 36.4 |

Table 6: **Performance (FPS) in each scene.** We measure the number of Gaussian kernels and physical particles

environment after object removal and the segmented targets, which achieves accurate boundary detection of the targets. This significantly benefits the dynamic scenes and geometry-related processing in various scenarios. However, despite the robustness of our imported grouping loss, our method still relies on the generated masks especially in *mask stage*. If significant occlusion or tracking loss exists in the dataset, it can negatively affect the results of the mask stage, which may require more adjustments to fix, such as threshold modifications.

Material Analysis. In our experiments, we find that GPT-4o can be extremely accurate in category recognition. Given one or two views with precise mask to indicate the target, it can handle complex situation such as distinguishing between the container and its content. Besides, it can refer to the analysis history in the same scene, which ensures the relative accuracy. For example, the biggest cushion is recognized as the heaviest in *sofa* dataset. When combined with Gaussian kernels, we utilize the explicit representations of GS to generate our correction factor, which works well when eliminating the effect of distance. However, it is hard to predict the absolute value directly without reference, which may cause fake analysis, especially across different scenes. For example, the doll wolf (in *wolf* dataset) should not have such great *plasticity* compared with pillows (in *sofa* dataset). Although it is difficult for users to notice this, there is still room for improvement.

Physical Simulation. We develop a unified simulation framework based on PBD, which uses a uniform interpolation method for various physical simulation such as plastic and elastic deformation, fracture in rigid and granular material. Our method connects the Gaussian kernels and physical particles with unified representations, enabling various physical-based tasks in GS reconstructed scenes. Besides, Our method balances the real-time performance and physical simulation realism, thus supporting the applications in VR. This particle generation strategy ensures the computational complexity related with the volume or surface of the target, instead of the kernel number. On public datasets, we live up to the demand of interactive VR applications, reaching almost 60 FPS. Even in our most complicated scene with multiple simulation targets, we can reach 36 FPS.

Despite the mentioned advantages, we find some limitations in our simulation. For granular material, the particles easily clip through the containers, which is also the drawbacks of PBD. Although shortening the time step can address this issue to some extent, it also leads to significant calculation overload. For fracture, the inside kernels can expose due to the division and rotation of particles, which can generate blurry rendering effects. Our subsequent work may focus on processing of dynamic details and consistency between rendering and simulation.

6 CONCLUSION

In this paper, we presented LIVE-GS, a highly realistic interactive GS-based VR system with advanced scene understanding capabilities powered by LLM. From few input images, our system enhances the scene by analyzing the physical properties of each element and tracking possible artifacts when reconstructing the scenes. Even when faced with complex real-world data, LIVE-GS enables de-

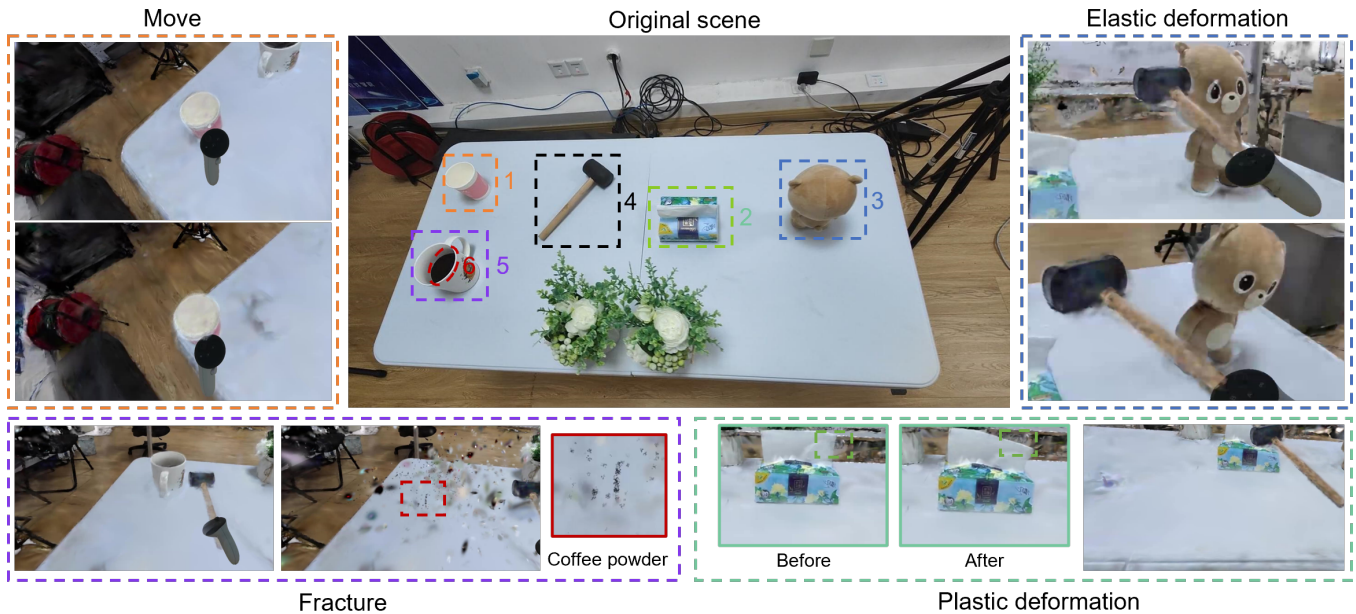


Figure 12: **Interaction in our custom dataset labdesk.** From one to six are respectively a paper cup, a box of tissues, a Teddy Bear, a plastic hammer, a mug and coffee powder in the mug. After segmentation and analysis, we hold the hammer and interact with other objects in our demo.

tailed reconstruction and segmentation, integrating various physical simulations for real-time interaction consistent with visual effects. Our work reveals the potential of the combination of 3DGS and LLM in dynamic scene reconstructions and interactions, which could become a mainstream method for future VR asset creation.

REFERENCES

- [1] J. Bae, S. Kim, Y. Yun, H. Lee, G. Bang, and Y. Uh. Per-gaussian embedding-based deformation for deformable 3d gaussian splatting. *arXiv preprint arXiv:2404.03613*, 2024. 2
- [2] J. Cen, J. Fang, C. Yang, L. Xie, X. Zhang, W. Shen, and Q. Tian. Segment any 3d gaussians, 2024. 2
- [3] H. K. Cheng, S. W. Oh, B. Price, A. Schwing, and J.-Y. Lee. Tracking anything with decoupled video segmentation. In *Proceedings of the IEEE/CVF International Conference on Computer Vision*, pp. 1316–1326, 2023. 2, 3, 5
- [4] W.-H. Chu, L. Ke, and K. Fragkiadaki. Dreamscene4d: Dynamic multi-object scene generation from monocular videos. *arXiv preprint arXiv:2405.02280*, 2024. 2
- [5] N. Deng, Z. He, J. Ye, B. Duinkharjav, P. Chakravarthula, X. Yang, and Q. Sun. Fov-nerf: Foveated neural radiance fields for virtual reality. *IEEE Transactions on Visualization and Computer Graphics*, 28(11):3854–3864, 2022. 1
- [6] R. Ding, J. Yang, C. Xue, W. Zhang, S. Bai, and X. Qi. Pla: Language-driven open-vocabulary 3d scene understanding. In *Proceedings of the IEEE/CVF conference on computer vision and pattern recognition*, pp. 7010–7019, 2023. 2
- [7] B. Dou, T. Zhang, Y. Ma, Z. Wang, and Z. Yuan. Cosseggaussians: Compact and swift scene segmenting 3d gaussians. *arXiv preprint arXiv:2401.05925*, 2024. 2
- [8] B. P. Duisterhof, Z. Mandi, Y. Yao, J.-W. Liu, M. Z. Shou, S. Song, and J. Ichnowski. Md-splatting: Learning metric deformation from 4d gaussians in highly deformable scenes. *arXiv preprint arXiv:2312.00583*, 2023. 2
- [9] L. Fan, Y. Yang, M. Li, H. Li, and Z. Zhang. Trim 3d gaussian splatting for accurate geometry representation. *arXiv preprint arXiv:2406.07499*, 2024. 2
- [10] A. Geiger, S. Gao, A. Chen, Z. Yu, and B. Huang. 2d gaussian splatting for geometrically accurate radiance fields. 2024. 2
- [11] R. Girdhar, A. El-Nouby, Z. Liu, M. Singh, K. V. Alwala, A. Joulin, and I. Misra. Imagebind: One embedding space to bind them all. In *Proceedings of the IEEE/CVF Conference on Computer Vision and Pattern Recognition*, pp. 15180–15190, 2023. 2
- [12] S. Guan, H. Deng, Y. Wang, and X. Yang. Neurofluid: Fluid dynamics grounding with particle-driven neural radiance fields. In *International Conference on Machine Learning*, pp. 7919–7929. PMLR, 2022. 2
- [13] A. Guédon and V. Lepetit. Sugar: Surface-aligned gaussian splatting for efficient 3d mesh reconstruction and high-quality mesh rendering. In *Proceedings of the IEEE/CVF Conference on Computer Vision and Pattern Recognition*, pp. 5354–5363, 2024. 2
- [14] Z. Guo, W. Zhou, L. Li, M. Wang, and H. Li. Motion-aware 3d gaussian splatting for efficient dynamic scene reconstruction. *arXiv preprint arXiv:2403.11447*, 2024. 2
- [15] X. Hu, Y. Wang, L. Fan, J. Fan, J. Peng, Z. Lei, Q. Li, and Z. Zhang. Semantic anything in 3d gaussians. *arXiv preprint arXiv:2401.17857*, 2024. 2, 4
- [16] J. Huang, H. Yu, J. Zhang, and H. Nait-Charif. Point’n move: Interactive scene object manipulation on gaussian splatting radiance fields. *IET Image Processing*, 2023. 2
- [17] Y.-H. Huang, Y.-T. Sun, Z. Yang, X. Lyu, Y.-P. Cao, and X. Qi. Scgs: Sparse-controlled gaussian splatting for editable dynamic scenes. In *Proceedings of the IEEE/CVF Conference on Computer Vision and Pattern Recognition*, pp. 4220–4230, 2024. 2
- [18] C. Jia, Y. Yang, Y. Xia, Y.-T. Chen, Z. Parekh, H. Pham, Q. Le, Y.-H. Sung, Z. Li, and T. Duerig. Scaling up visual and vision-language representation learning with noisy text supervision. In *International conference on machine learning*, pp. 4904–4916. PMLR, 2021. 2
- [19] Y. Jiang, C. Yu, T. Xie, X. Li, Y. Feng, H. Wang, M. Li, H. Lau, F. Gao, Y. Yang, et al. Vr-gs: A physical dynamics-aware interactive gaussian splatting system in virtual reality. *arXiv preprint arXiv:2401.16663*, 2024. 2, 5
- [20] L. Kavan, S. Collins, J. Žára, and C. O’Sullivan. Skinning with dual quaternions. In *Proceedings of the 2007 symposium on Interactive 3D graphics and games*, pp. 39–46, 2007. 2
- [21] B. Kerbl, G. Kopanas, T. Leimkühler, and G. Drettakis. 3d gaussian

- splatting for real-time radiance field rendering. *ACM Transactions on Graphics*, 42(4):1–14, 2023. 1, 2, 3
- [22] A. Kirillov, E. Mintun, N. Ravi, H. Mao, C. Rolland, L. Gustafson, T. Xiao, S. Whitehead, A. C. Berg, W.-Y. Lo, et al. Segment anything. In *Proceedings of the IEEE/CVF International Conference on Computer Vision*, pp. 4015–4026, 2023. 2, 3
- [23] X. Li, Y.-L. Qiao, P. Y. Chen, K. M. Jatavallabhula, M. Lin, C. Jiang, and C. Gan. Pac-nerf: Physics augmented continuum neural radiance fields for geometry-agnostic system identification. *arXiv preprint arXiv:2303.05512*, 2023. 2
- [24] H. Liang, Y. Yin, D. Xu, H. Liang, Z. Wang, K. N. Plataniotis, Y. Zhao, and Y. Wei. Diffusion4d: Fast spatial-temporal consistent 4d generation via video diffusion models. *arXiv preprint arXiv:2405.16645*, 2024. 2
- [25] G. Liao, J. Li, Z. Bao, X. Ye, J. Wang, Q. Li, and K. Liu. Clip-gs: Clip-informed gaussian splatting for real-time and view-consistent 3d semantic understanding. *arXiv preprint arXiv:2404.14249*, 2024. 2
- [26] G. Liao, K. Zhou, Z. Bao, K. Liu, and Q. Li. Ov-nerf: Open-vocabulary neural radiance fields with vision and language foundation models for 3d semantic understanding. *arXiv preprint arXiv:2402.04648*, 2024. 2
- [27] Z. Liu, H. Ouyang, Q. Wang, K. L. Cheng, J. Xiao, K. Zhu, N. Xue, Y. Liu, Y. Shen, and Y. Cao. Infusion: Inpainting 3d gaussians via learning depth completion from diffusion prior. *arXiv preprint arXiv:2404.11613*, 2024. 2
- [28] M. Loper, N. Mahmood, J. Romero, G. Pons-Moll, and M. J. Black. Smpl: A skinned multi-person linear model. In *Seminal Graphics Papers: Pushing the Boundaries, Volume 2*, pp. 851–866, 2023. 2
- [29] T. Lu, M. Yu, L. Xu, Y. Xiangli, L. Wang, D. Lin, and B. Dai. Scaffold-gs: Structured 3d gaussians for view-adaptive rendering. In *Proceedings of the IEEE/CVF Conference on Computer Vision and Pattern Recognition*, pp. 20654–20664, 2024. 2
- [30] Y. Lu, C. Xu, X. Wei, X. Xie, M. Tomizuka, K. Keutzer, and S. Zhang. Open-vocabulary point-cloud object detection without 3d annotation. In *Proceedings of the IEEE/CVF conference on computer vision and pattern recognition*, pp. 1190–1199, 2023. 2
- [31] B. Mildenhall, P. P. Srinivasan, M. Tancik, J. T. Barron, R. Ramamoorthi, and R. Ng. Nerf: Representing scenes as neural radiance fields for view synthesis. *Communications of the ACM*, 65(1):99–106, 2021. 1
- [32] M. Müller, B. Heidelberg, M. Hennix, and J. Ratcliff. Position based dynamics. *Journal of Visual Communication and Image Representation*, 18(2):109–118, 2007. 2, 5
- [33] T. Müller, A. Evans, C. Schied, and A. Keller. Instant neural graphics primitives with a multiresolution hash encoding. *ACM transactions on graphics (TOG)*, 41(4):1–15, 2022. 6
- [34] S. Peng, K. Genova, C. Jiang, A. Tagliasacchi, M. Pollefeys, T. Funkhouser, et al. Openscene: 3d scene understanding with open vocabularies. In *Proceedings of the IEEE/CVF conference on computer vision and pattern recognition*, pp. 815–824, 2023. 2
- [35] Y.-L. Qiao, A. Gao, and M. Lin. Neuphysics: Editable neural geometry and physics from monocular videos. *Advances in Neural Information Processing Systems*, 35:12841–12854, 2022. 2
- [36] M. Qin, W. Li, J. Zhou, H. Wang, and H. Pfister. Langsplat: 3d language gaussian splatting. In *Proceedings of the IEEE/CVF Conference on Computer Vision and Pattern Recognition*, pp. 20051–20060, 2024. 2
- [37] R.-Z. Qiu, G. Yang, W. Zeng, and X. Wang. Feature splatting: Language-driven physics-based scene synthesis and editing. *arXiv preprint arXiv:2404.01223*, 2024. 2
- [38] A. Radford, J. W. Kim, C. Hallacy, A. Ramesh, G. Goh, S. Agarwal, G. Sastry, A. Askell, P. Mishkin, J. Clark, et al. Learning transferable visual models from natural language supervision. In *International conference on machine learning*, pp. 8748–8763. PMLR, 2021. 2
- [39] J. Ren, L. Pan, J. Tang, C. Zhang, A. Cao, G. Zeng, and Z. Liu. Dreamgaussian4d: Generative 4d gaussian splatting. *arXiv preprint arXiv:2312.17142*, 2023. 2
- [40] K. Ren, L. Jiang, T. Lu, M. Yu, L. Xu, Z. Ni, and B. Dai. Octree-gs: Towards consistent real-time rendering with lod-structured 3d gaussians. *arXiv preprint arXiv:2403.17898*, 2024. 2
- [41] J.-C. Shi, M. Wang, H.-B. Duan, and S.-H. Guan. Language embedded 3d gaussians for open-vocabulary scene understanding. In *Proceedings of the IEEE/CVF Conference on Computer Vision and Pattern Recognition*, pp. 5333–5343, 2024. 2
- [42] Y. Siddiqui, L. Porzi, S. R. Buló, N. Müller, M. Nießner, A. Dai, and P. Kotschieder. Panoptic lifting for 3d scene understanding with neural fields. In *Proceedings of the IEEE/CVF Conference on Computer Vision and Pattern Recognition*, pp. 9043–9052, 2023. 2
- [43] M. C. Silva, M. Dahaghin, M. Toso, and A. Del Bue. Contrastive gaussian clustering: Weakly supervised 3d scene segmentation. *arXiv preprint arXiv:2404.12784*, 2024. 2
- [44] N. Snavely, S. M. Seitz, and R. Szeliski. Photo tourism: exploring photo collections in 3d. In *ACM siggraph 2006 papers*, pp. 835–846, 2006. 3
- [45] R. Suvorov, E. Logacheva, A. Mashikhin, A. Remizova, A. Ashukha, A. Silvestrov, N. Kong, H. Goka, K. Park, and V. Lempitsky. Resolution-robust large mask inpainting with fourier convolutions. In *Proceedings of the IEEE/CVF winter conference on applications of computer vision*, pp. 2149–2159, 2022. 2, 4
- [46] A. Takmaz, E. Fedele, R. W. Sumner, M. Pollefeys, F. Tombari, and F. Engelmann. Openmask3d: Open-vocabulary 3d instance segmentation. *arXiv preprint arXiv:2306.13631*, 2023. 2
- [47] O. S. D. Team. Obi solver. <https://obi.virtualmethodstudio.com/>, 2024. 5
- [48] O. Topsakal and T. C. Akinci. Creating large language model applications utilizing langchain: A primer on developing llm apps fast. In *International Conference on Applied Engineering and Natural Sciences*, vol. 1, pp. 1050–1056, 2023. 5
- [49] M. Turkulainen, X. Ren, I. Melekhov, O. Seiskari, E. Rahtu, and J. Kannala. Dn-splatter: Depth and normal priors for gaussian splatting and meshing. *arXiv preprint arXiv:2403.17822*, 2024. 2
- [50] J. Wang, J. Fang, X. Zhang, L. Xie, and Q. Tian. Gaussianeditor: Editing 3d gaussians delicately with text instructions. In *Proceedings of the IEEE/CVF Conference on Computer Vision and Pattern Recognition*, pp. 20902–20911, 2024. 2
- [51] Y. Wolf, A. Bracha, and R. Kimmel. Surface reconstruction from gaussian splatting via novel stereo views. *arXiv preprint arXiv:2404.01810*, 2024. 2
- [52] T. Xie, Z. Zong, Y. Qiu, X. Li, Y. Feng, Y. Yang, and C. Jiang. Physgaussian: Physics-integrated 3d gaussians for generative dynamics. In *Proceedings of the IEEE/CVF Conference on Computer Vision and Pattern Recognition*, pp. 4389–4398, 2024. 2, 3, 5, 6
- [53] L. Xu, V. Agrawal, W. Laney, T. Garcia, A. Bansal, C. Kim, S. Rota Buló, L. Porzi, P. Kotschieder, A. Božič, et al. Vr-nerf: High-fidelity virtualized walkable spaces. In *SIGGRAPH Asia 2023 Conference Papers*, pp. 1–12, 2023. 1
- [54] S. Yan, T. Zhu, Z. Wang, Y. Cao, M. Zhang, S. Ghosh, Y. Wu, and J. Yu. Videococa: Video-text modeling with zero-shot transfer from contrastive captioners. *arXiv preprint arXiv:2212.04979*, 2022. 2
- [55] Z. Yang, X. Gao, W. Zhou, S. Jiao, Y. Zhang, and X. Jin. Deformable 3d gaussians for high-fidelity monocular dynamic scene reconstruction. In *Proceedings of the IEEE/CVF Conference on Computer Vision and Pattern Recognition*, pp. 20331–20341, 2024. 2
- [56] M. Ye, M. Danelljan, F. Yu, and L. Ke. Gaussian grouping: Segment and edit anything in 3d scenes. *arXiv preprint arXiv:2312.00732*, 2023. 2, 3, 5
- [57] Y. Yin, D. Xu, Z. Wang, Y. Zhao, and Y. Wei. 4dgen: Grounded 4d content generation with spatial-temporal consistency. *arXiv preprint arXiv:2312.17225*, 2023. 2
- [58] Y.-J. Yuan, Y.-T. Sun, Y.-K. Lai, Y. Ma, R. Jia, and L. Gao. Nerf-editing: geometry editing of neural radiance fields. In *Proceedings of the IEEE/CVF Conference on Computer Vision and Pattern Recognition*, pp. 18353–18364, 2022. 2
- [59] A. Zeng, M. Attarian, B. Ichter, K. Choromanski, A. Wong, S. Welker, F. Tombari, A. Purohit, M. Ryoo, V. Sindhwani, et al. Socratic models: Composing zero-shot multimodal reasoning with language. *arXiv preprint arXiv:2204.00598*, 2022. 2
- [60] H. Zhang, F. Li, S. Liu, L. Zhang, H. Su, J. Zhu, L. M. Ni, and H.-Y. Shum. Dino: Detr with improved denoising anchor boxes for end-to-end object detection. *arXiv preprint arXiv:2203.03605*, 2022. 2
- [61] H. Zhang, X. Li, and L. Bing. Video-llama: An instruction-tuned

audio-visual language model for video understanding. *arXiv preprint arXiv:2306.02858*, 2023. 2

- [62] T. Zhang, H.-X. Yu, R. Wu, B. Y. Feng, C. Zheng, N. Snavely, J. Wu, and W. T. Freeman. Physdreamer: Physics-based interaction with 3d objects via video generation. *arXiv preprint arXiv:2404.13026*, 2024. 2, 4
- [63] S. Zhi, T. Laidlow, S. Leutenegger, and A. J. Davison. In-place scene labelling and understanding with implicit scene representation. In *Proceedings of the IEEE/CVF International Conference on Computer Vision*, pp. 15838–15847, 2021. 2
- [64] H. Zhou, J. Shao, L. Xu, D. Bai, W. Qiu, B. Liu, Y. Wang, A. Geiger, and Y. Liao. Hugs: Holistic urban 3d scene understanding via gaussian splatting. In *Proceedings of the IEEE/CVF Conference on Computer Vision and Pattern Recognition*, pp. 21336–21345, 2024. 2
- [65] M. Zwicker, H. Pfister, J. Van Baar, and M. Gross. Ewa volume splatting. In *Proceedings Visualization, 2001. VIS'01.*, pp. 29–538. IEEE, 2001. 3